scientific reports

OPEN

Intelligent modeling and optimization of titanium surface etching for dental implant application

Seyyed Mohamad Sadati Tilebon[1], Seyed Amirhossein Emamian[2], Hosseinali Ramezanpour[2], Hashem Yousefi[2], Mutlu Özcan[3], Seyed Morteza Naghib[4 ✉], Yasser Zare[5] & Kyong Yop Rhee[5]

Acid-etching is one of the most popular processes for the surface treatment of dental implants. In this paper, acid-etching of commercially pure titanium (cpTi) in a 48% H_2SO_4 solution is investigated. The etching process time (0–8 h) and solution temperature (25–90 °C) are assumed to be the most effective operational conditions to affect the surface roughness parameters such as arithmetical mean deviation of the assessed profile on the surface (R_a) and average of maximum peak to valley height of the surface over considered length profile (R_z), as well as weight loss (WL) of the dental implants in etching process. For the first time, three multilayer perceptron artificial neural network (MLP-ANN) with two hidden layers was optimized to predict R_a, R_z, and WL. MLP is a feedforward class of ANN and ANN model that involves computations and mathematics which simulate the human–brain processes. The ANN models can properly predict R_a, R_z, and WL variations during etching as a function of process temperature and time. Moreover, WL can be increased to achieve a high Ra. At WL = 0, R_a of 0.5 μm is obtained, whereas R_a increases to 2 μm at WL = 0.78 μg/cm². Also, ANN model was fed into a nonlinear sorting genetic algorithm (NSGA-II) to establish the optimization process and the ability of this method has been proven to predict the optimized etching conditions.

Creating rough surfaces on medical implants has been shown to improve their bio-integration resulting from increased bone tissue production at the modified surfaces[1–4]. Many studies have shown that undesirable fibrous tissues tend to form on smooth surfaces, while rougher surfaces promote the formation of solid bone tissue[5,6] conducted a long-term study of bone integration with implants[7,8]. Bone is generated in a multistep process wherein osteoclast cells selectively remove tissue to form pits (lacunae), and the osteoblast cells, in turn, collect and form the bone matrix tissues[9]. As osteoclasts cannot interact with implant materials, such as titanium (Ti), osteoblast bonding can be inhibited if an implant's surface does not possess micro-, meso-, ornano-scale structures similar to those created by osteoclasts[10].

Usually, surface roughness is checked with some parameters like R_a, R_z, and S_a. R_a is a 1-D parameter and is defined as arithmetical mean deviation of the assessed profile[11]. For measurement of R_a, a very thin detector tip moves in a horizontal linear direction over the surface of the sample (in contact or noncontact mode), that vertical moves will be reported[12,13]. R_z is maximum peak to valley height of the same profile, that is studied for R_a measurement[12]. S_a is an areal roughness parameter that is detected from a 2-D surface (unlike Ra that is detected from a linear path)[11]. Based on definitions, R_a and S_a are very close to each other and choosing one of them is based on measurement equipment (some of them report R_a and some other report S_a)[11,12].

Etching is one of the most popular processes used to enhance surface roughness and improve other properties of the surface. It is responsible for enhancing a dental implant's contact with bone and can specify the strength of the implant's contact with the surface[11–15] and bone response[16–20]. Currently, a wide range of commercial dental implants is available in the market. These implants have differing properties, such as the implant's core, geometric specifications, and surface characteristics. Some commercial brands, such as Ospol (Hollviken, Sweden), with

[1]Surface Engineering Unit, AVITA Dental System, KFP-Dental Company, Tehran, Iran. [2]Research and Development Unit, AVITA Dental System, KFP-Dental Company, Tehran, Iran. [3]Division of Dental Biomaterials, Center for Dental and Oral Medicine, Clinic for Reconstructive Dentistry, University of Zürich, Zurich, Switzerland. [4]Nanotechnology Department, School of Advanced Technologies, Iran University of Science and Technology, P.O. Box 16846-13114, Tehran, Iran. [5]Department of Mechanical Engineering, College of Engineering, Kyung Hee University, Yongin 446-701, Republic of Korea. ✉email: naghib@iust.ac.ir

$S_a = 0.26$ μm, have a smooth surface ($S_a < 1$ μm is considered smooth)[21]. On the other hand, other commercial implants, such as SLA (Standard Plus; ITI Straumann, Basel, Switzerland; $S_a = 1.7$ μm), Ankylos (Dentsply-Friadent, Menheim, Germany; $S_a = 1.55$ μm), Frialit (DentsplyFriadent, Menheim, Germany; $S_a = 1.79$ μm), and Promote (Screwline, calmog, Basel, Switzerland; $S_a = 1.30$ μm), are moderately rough (with S_a in the range of 1–2 μm)[22,23]. Additionally, some other surfaces, such as the Kohno HRPS and Kohno DES HRPS (Sweden & Martina, Due Carrare, Italy; $S_a = 3.11$ and 3.16 respectively), have the highest degree of roughness (surfaces with $S_a > 2$ are considered maximally rough)[22,23].

In 2010, Elias[24] reported that acid-etched implants have a more homogeneous surface compared to machined surfaces. In addition, the acid etching process, when applied as a pretreatment for anodizing the dental implants (or other processes), provides homogeneous roughness, a large active surface area, and improves bio-adhesion. Grizon and coworkers[25] conducted a long-term study to investigate the enhancement of bone-implant integration with increased surface roughness. No significant differences were observed for the two types of implants between 3–6 months. At 12 and 18 months, the bone volume and contact interface were still increasing, and the implants with $R_a = 0.206$ μm were associated with higher values than the smoother implants ($R_a = 0.160$). Many similar studies, such as one by Fouziya et al.[26] reported that, smoother surfaces require a longer time for osseointegration and prosthetic loading.

The trends in dental implant surface modifications can be classified into the five generations shown in Fig. 1a. Etching was part of the first generation of methods for improving machined surfaces with mechanical treatment. Despite all the improvements to surface modification methods, etching is still widely used in commercial systems, either directly as a final surface modification or in combination with other methods. Based on Fig. 1b, after the plasma spray coating process, etching, with a more than 15% usage rate, is the second most used method based on published reports. In addition, several of the other methods, like sandblasting and sandblasting plus acid etching (SLA), use etching as a treatment method[27].

Acid etched has a lower risk of implant surface contamination than blasting since there are no particle remnants on the surface[28]. This surface enhances the migration and retention of osteogenic cells. There are variations in acid etching methods between the different manufacturers based on acid concentration, process time, and temperatures. Acid etching forms micropits on the implant surface[29] and titanium hydrides that are replaced by oxygen, slowing the transformation of the implant surface. In addition, nanosized titanium particles are formed on the surface that favor the adhesion of proteins through surface nano-roughness features[30]. Acid-etched surfaces show more bone apposition, increasing the interfacial strength as calculated by removal torque[31–33] or push-out tests[14,34]. Moreover, etching the dental implant surfaces leads to a reduction in the healing time in the mandible and the maxilla at 6–8 weeks (from 3–6 months)[35–38].

Mathematical models for etching process can lead to choosing suitable operation condition and having desirable surface for dental implants. Between different methods of modelling, artificial neural networks (ANN) have many advantages over others and intelligent modelling using experimental datasets for model configuration have more reliability. ANNs are a technology based on the studies of the nervous system and brain. These networks emulate a biological neural network but they use a reduced set of concepts from biological neural systems. Specifically, ANN models simulate the electrical activity of the brain and nervous system. Processing elements (also known as either a neuron or perceptron) are connected to other processing elements. Typically, the neuron is arranged in a layer or vector with the output of one layer, serving as the input to the next layer and possibly other layers. A neuron may be connected to all or a subset of the neuron in the subsequent layer. Weighted data signals entering a neuron simulate the electrical excitation of a nerve cell and consequently, the transference of information within the network or brain. Output of this data transfer between neurons, is processing on the data and prediction of output. ANN model should be optimized by training, validation and test[39–42]. Despite all advantages of ANN, a reliable model is needed to correct experimental datasets and collection of suitable data in appropriate number, that is costly and time consuming.

Numerical study of surface characteristics for dental implant application, is relatively new field of study. In 2020, Kohler et al.[43] reported a numerical model for titanium acid etching. Their model assumed R_a to be the only determining parameter. Weight loss as a parameter of geometrical limitations should be fixed in an acceptable range (based on quality control protocols). Intelligent modeling with artificial neural networks (ANN) can address the drawbacks of the other methods of modelling such as the inability to fit large amounts of data. Therefore, multilayer perceptron (MLP) ANN is used to model the etching process in 48% H_2SO_4 solution. In the following, nonlinear sorting genetic algorithm (NSGA-II) optimization method is utilized to arrive at the optimal conditions for the process.

Materials and methods

In this study, MLP-ANN was used to investigate the surface characteristics including the R_a, R_z, and WL when etching solution temperature and etching process time varies. A MLP-ANN with two hidden layers was used for achievement to the optimized topology of ANN, 1 to 5 neurons were tested in each hidden layer. Finally, ANN structure with lowest MSE was proposed as the best ANN model and fed to the NSGA-II for process optimization.

Ban et al.[44] investigated etching time and etching solution media temperature effects on surface characteristics. Data were feeding into ANN models. The following equation [Eq. (1)] was used to normalize input variables in rang of [−1, +1]:

$$X_i = 2 \times \frac{x_i - x_{min}}{x_{max} - x_{min}} - 1, \tag{1}$$

where Xi is a normalized value of input variable xi, x_{min} is minimum value of target functions and x_{max} is the maximum one[39,45].
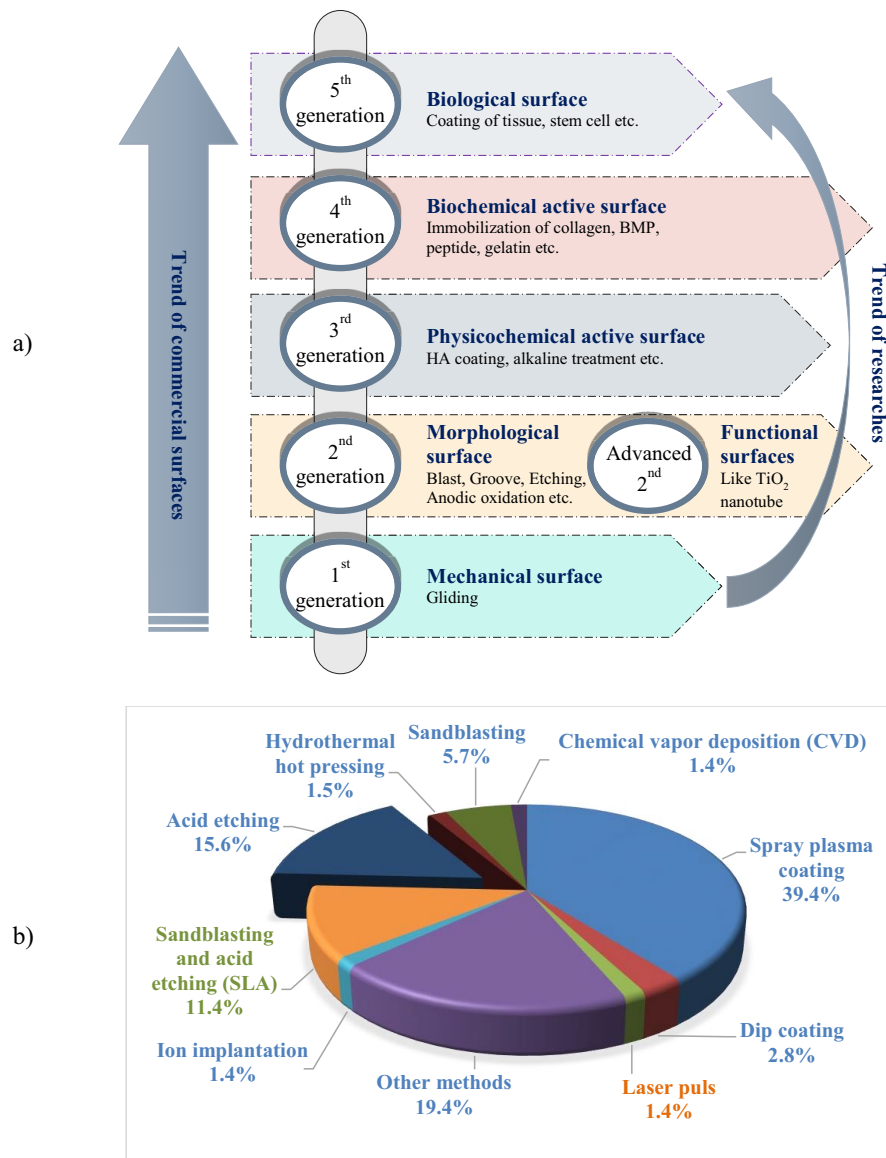
Figure 1. (**a**) Different generations of dental implant surface modifications, and (**b**) commonly used surface modification methods for titanium-based dental implants.

An in-house computational code was developed in this study that can conceptually search for best ANN configurations with dividing data into 'training', 'validation', and 'test' sets. Accordingly, 70% of data was randomly chosen to train the model. On the other hand, 15% of data was fed to ANN model for validation. Finally, the rest of the data was used for testing the configured ANN structure. Although there is no rigid rule to find the appropriate number of neurons in the hidden layers, the complexity of the relationship between inputs and outputs plays a key role[46,47]. Different combinations of neurons (one to five neurons in each hidden layer) in two hidden layers were tested for choosing the best configuration with a minimized error. The function defined through Eq. (2) was applied in output, and hidden layers were used as activation transfer function[40,48]:

$$f(x) = \frac{e^x - e^{-x}}{e^x + e^{-x}}. \tag{2}$$

A well-organized in-house code based on the flowchart illustrated in Fig. 2 was used to model R_a, R_z, and WL (three different models). A gradient descent (G.D.) method was used to model optimization parameters and find the best biases and weights to match the input and output variables.

Number of neurons in hidden layer 1 and hidden layer 2 varied in range of 1 to 5 (max NH1 and max NH2 is equal to 5). Model accuracy for response prediction was measured by mean of squared error (MSE) criterion[49,50] as noted in Eq. (3)[39,46,47,51].
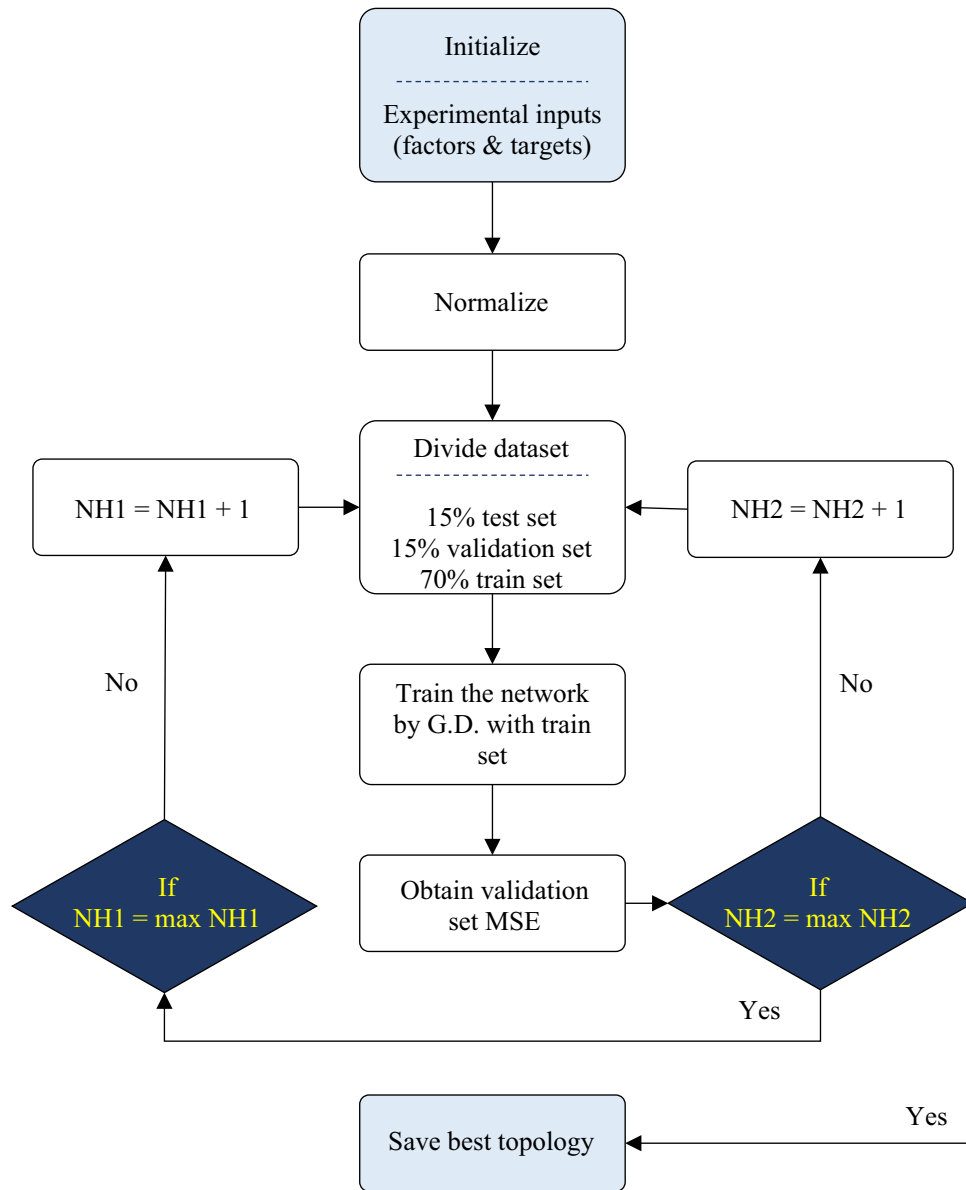
Figure 2. Modeling flowchart based on ANN method.

$$MSE = \frac{1}{n} \sum_{i=1}^{n} (Y_i - \overline{Y}_i)^2, \tag{3}$$

where n is the number of samples, Y_i and $\overline{Y}_i$ are experimental and predicted value of response for sample i.

To reach the desirable model the inputs must be normalized and also activation transfer function should be used for output and hidden layers. Several types of activation transfer function are utilized. Three of these functionsaremore important and applicable that shown in Fig. 3; Pureline [Eq. (4)], Logsig [Eq. (5)], and Tansig [Eq. (7)].

- Linear transfer function (Purelin)

$$f(x) = s \tag{4}$$

This transfer function is regularly employed in the output layer. The primary interest of MLPs resides in their nonlinear sigmoid function (such as logsig and tansig) principally used in their hidden layers.
- Log-Sigmoid transfer function (Logsig)
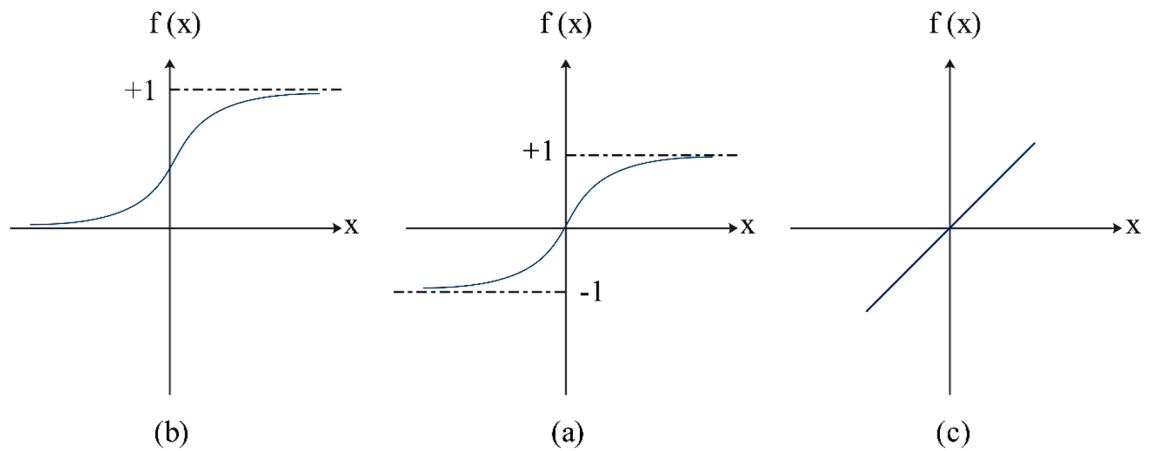
Figure 3. Typical transfer functions (**a**) Logsig, (**b**) Tansig, and (**c**) Pureline.

Optimization parameter	Value
Initial population size	25
Crossover mechanism	Arithmetic
Crossover rate	70%
Mutation mechanism	Polynomial
Mutation rate	40%
Selection mechanism	Ternary tournament selection
Maximum iteration number	50

Table 1. The values of parameters used for multi-objective optimization by G.A. approaches.

$$f(x) = \frac{1}{1 + e^{-x}},$$ (5)

which is easily differentiable, and frequently used as a nonlinear transfer function for engineering applications. However, because it is limited between 0 and 1, its linearly transformed type is used instead. It is recognized as the bipolar transfer function [Eq. (6)]:

$$f(x) = \frac{2}{1 + e^{-x}} - 1$$ (6)

- Hyperbolic Tangent Sigmoid (Tansig)

$$f(x) = \frac{e^x - e^{-x}}{e^x + e^{-x}},$$ (7)

which is very alike in kind and shares many mathematical properties with the bipolar transfer function and it is bounded between -1 and $+1$. It is too often employed in engineering application.

In the light of the above procedure, three ANN modelswere optimized to investigate the effective parameters on surface properties (R_a, R_z, and WL). In the next step, for the multi-objective optimization of the etching process in 48% H_2SO_4 solution, a Non-Dominated Sorting Genetic Algorithm-II (NSGA-II) was utilized. For the production of chromosomes, the value of each gene was randomly chosen in view of the values of variables given in Table 1. The code was then implemented to find the fitness of each chromosome to optimize surface properties simultaneously. After giving pairs of chromosomes were compared together, they were isolated from the remainder, as the first Pareto front. This operation was surveyed to obtain Pareto fronts 2, 3, etc. Pareto front n was assigned to the chromosome that has been dominated (n − 1) times. We also used crowding distance (C.D.) values, as the second criterion for optimization, was to sort pareto fronts [Eq. (8)]:

$$C.D.(i) = \sum_{x=1}^{N} \frac{d_e(i)}{\Delta_x(i)}$$ (8)

where $d_x(i) = |F_x(i+1) - F_x(i-1)|$ and $\Delta_x(i) = |\max F_x - \min F_x|$.

In Eq. (8), N is the number of objective functions, C.D. (i) is the crowding distance of the chromosome i, and $d_x(i)$ and $\Delta_x(i)$ are based on the objective function x, as shown in Fig. 4a. After estimating the degree of fitness
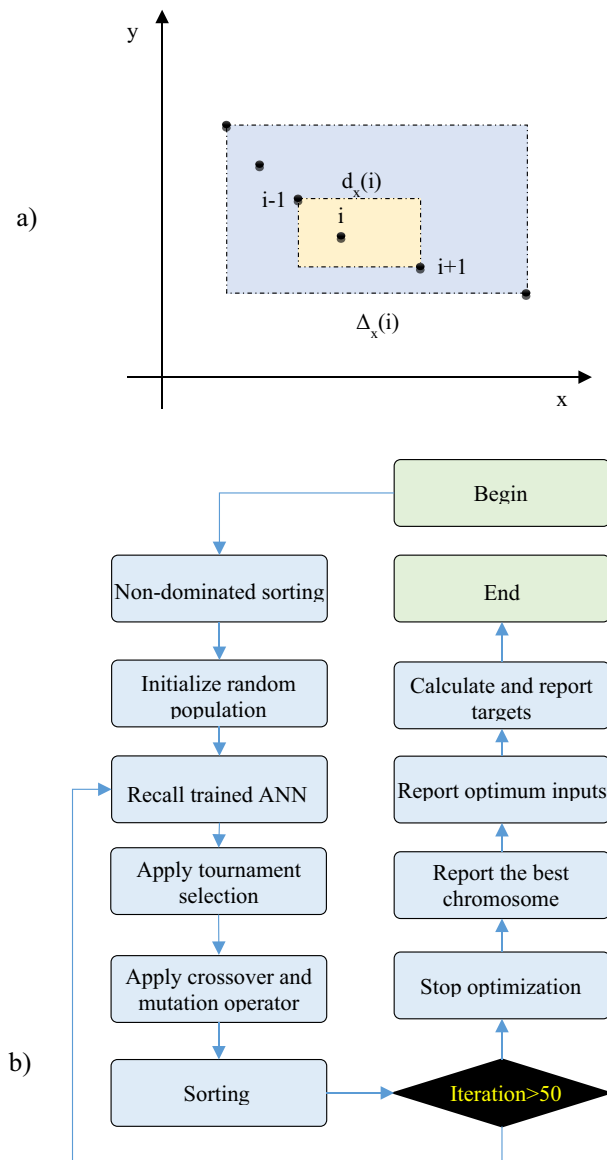
Figure 4. (**a**) Crowding distance calculation parameters for sample i, and (**b**) flowchart of NSGA-II based optimization.

based on primary and secondary constraints, chromosomes were sorted according to their favorability. The best chromosomes were chosen as the first Pareto front, followed by selecting, pairing, reproducing, and muting. The fitness of the parents and of the children of the new generation was revisited by utilizing a non-dominated sorting algorithm. Table 1 gives the values of parameters employed to optimizethesurface properties based on the NSGA-II evolutionary algorithm (Fig. 4b).

Results

ANN-based model evaluation.   *R_a ANN structure configuration and model validation.*   The ANN-based model evaluation for the R_a was completed in the first step. As shown in Fig. 5, an ANN model with two hidden layers (three neurons in the first hidden layer and one neuron in the second hidden layer) was the best structure for R_a prediction based on temperature (°C) and time (h) variation. Different combinations of Tansig and Logsig transfer functions were approved, and the results showed that the Tansig transfer function for both hidden layers performed best. The correlation coefficient (R) for the fixed ANN model, was 0.9892 that is very close to 1; this indicated that the model is reliable.

In the following, the accuracy of the model was studied by the quality line. As illustrated in section (a) of Fig. 6, the model fit is perfect if all the predicted data equals the experimental data. Therefore, the model has high accuracy if all data fall close to the y = x line. The ANN model predicted the experimental data with less than 10% error (see Fig. 6). As a result, the configured model was used to predict R_a under different operational
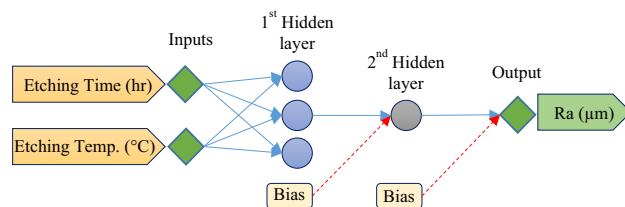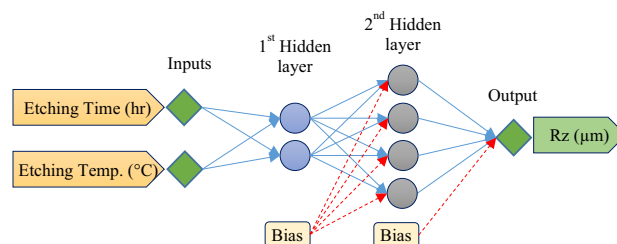
Figure 5. A schematic of the ANN model structure for R_a prediction based on etching time and etching ambient temperature.
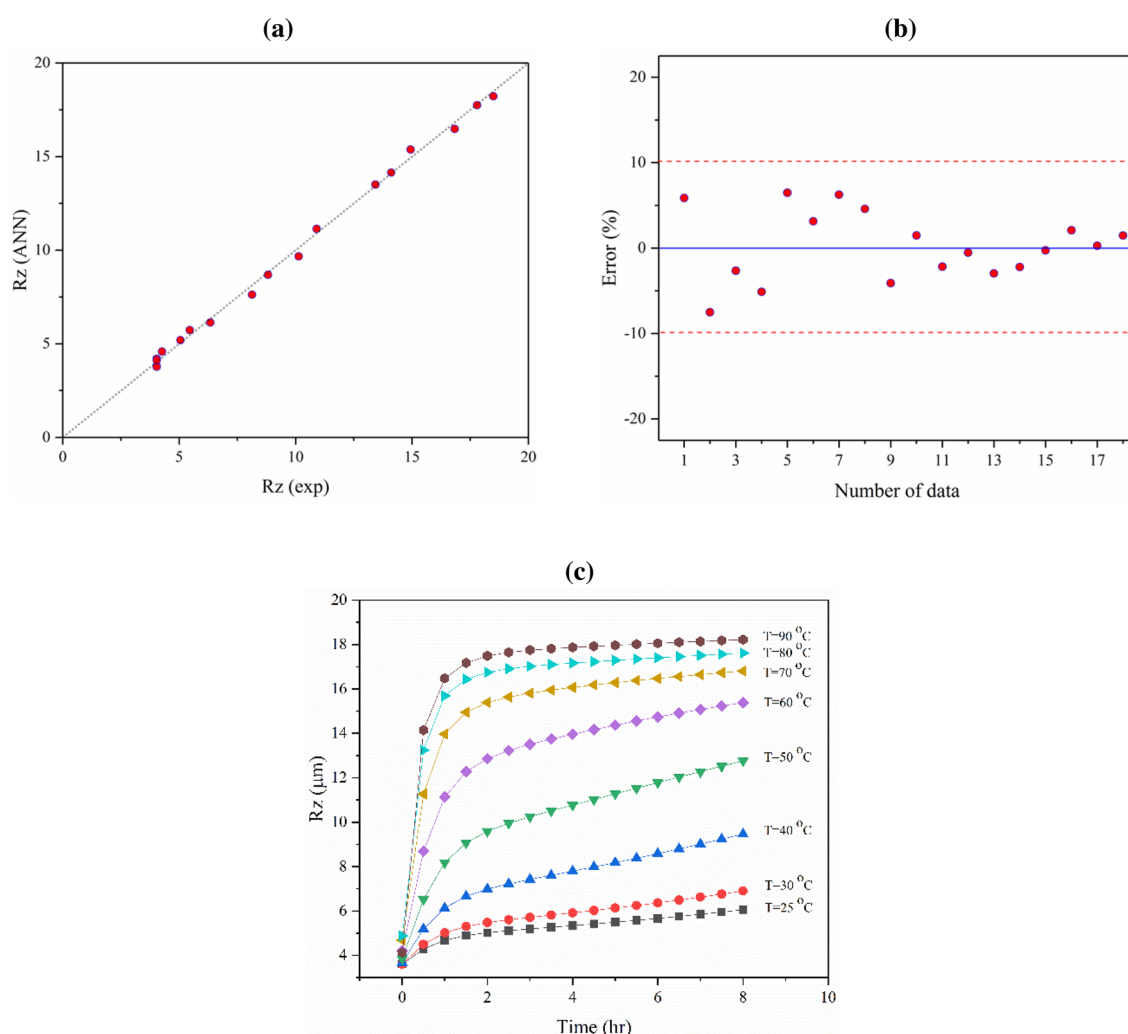
(a)

(b)

(c)
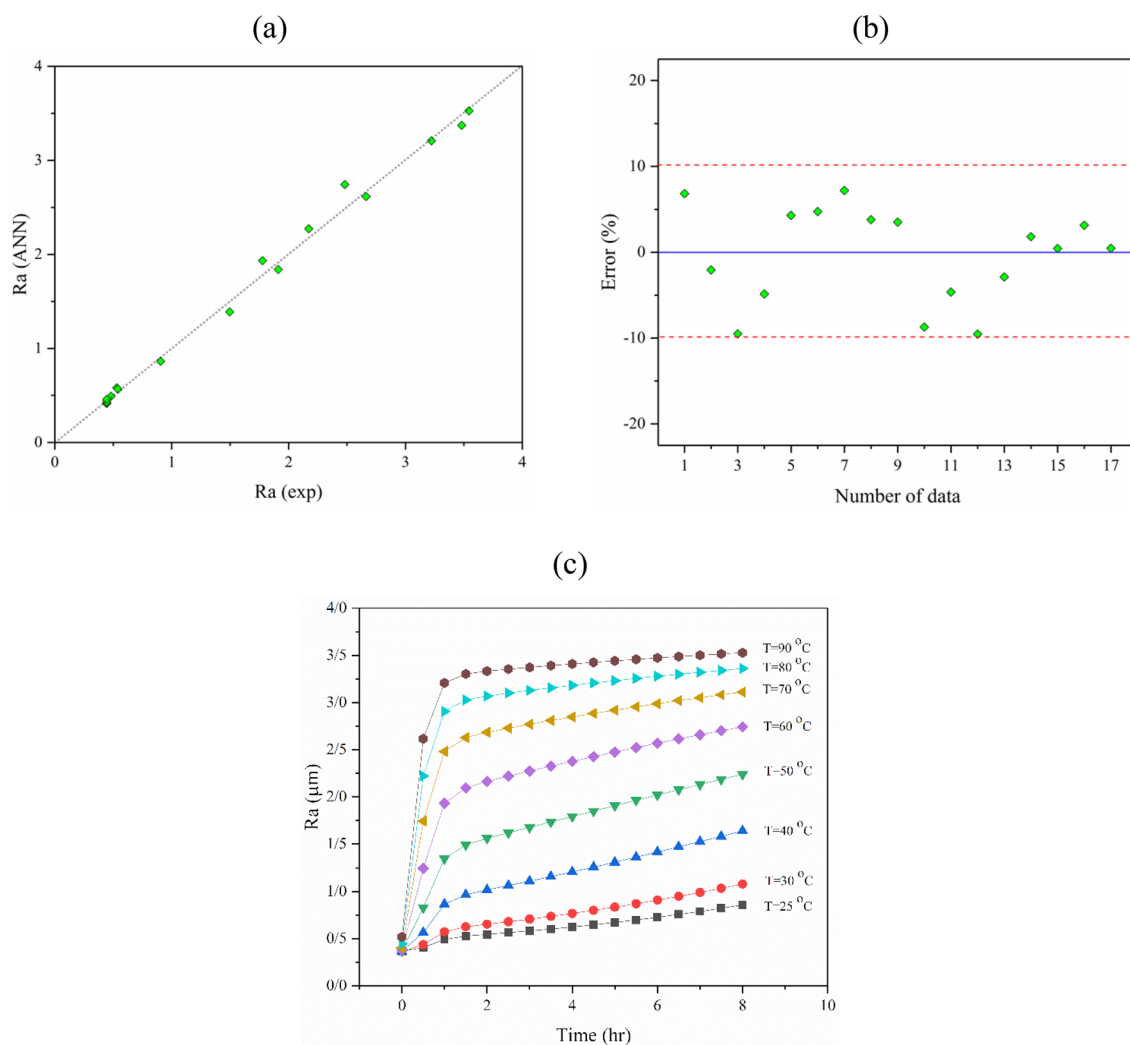
Figure 6. (**a**) Quality line, (**b**) the error values for experimental data and ANN model (R = 0.9892) outputs of R_a, and (**c**) the effect of time and temperature on the R_a of the titanium surface after etching with an H_2SO_4 etchant solution.

conditions in the time range of 0 to 8 h and different temperatures (25, 30, 40, 50, 60, 70, 80, and 90 °C), as presented in Fig. 6c.

R_z ANN structure configuration and model validation. The second ANN model was configured to predict R_z on the titanium surface during acid etching with 48% H_2SO_4 with etching time and solution temperature variation. The best ANN structure was obtained by an ANN model with two neurons and four neurons in the first and second hidden layers, respectively. The best transfer function for the first hidden layer was Logsig, while Tansig emerged as the best transfer function for the second hidden layer. A schematic structure of the optimized ANN model is presented in Fig. 7.

Figure 7. A schematic ANN model structure for R_z prediction based on etching time and solution temperature.
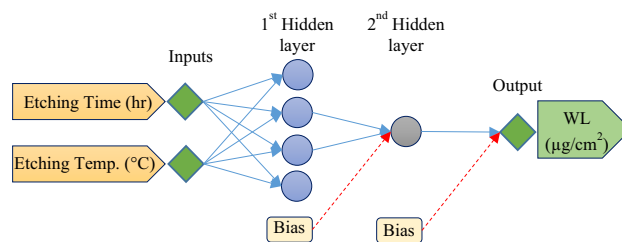

Figure 8. (**a**) Quality line, (**b**) the error values for experimental data and ANN model ($R = 9970$) outputs of R_z, and (**c**) the effect of time and temperature variation on the R_z of the titanium surface after etching with an H_2SO_4 etchant solution.

The ANN model accuracy for R_z prediction was further evaluated by calculating R, error, and the quality line. The optimized ANN model for R_z prediction had a correlation coefficient of about 0.9970. The quality line and error diagram showed that the chosen ANN model predicted the experimental data with suitable accuracy (see Fig. 8a,b). As shown in the error diagram, all data was predicted with minimal error (less than 10%). The validated model was then used to calculate R_z under different conditions. The pattern of R_z variation based on etching time in different etching media temperatures (25, 30, 40, 50, 60, 70, 80, and 90 °C) is shown in Fig. 8c.

WL ANN structure configuration and model validation. The ANN model was configured for experimental WL data during the etching of titanium in 48% H_2SO_4. In this step, an ANN model with four neurons in hidden layer 1 and one neuron in hidden layer 2 achieved the best topology, where Tansig-Tansig was the combina-

Figure 9. A schematic ANN model structure for WL prediction based on etching time and solution temperature.
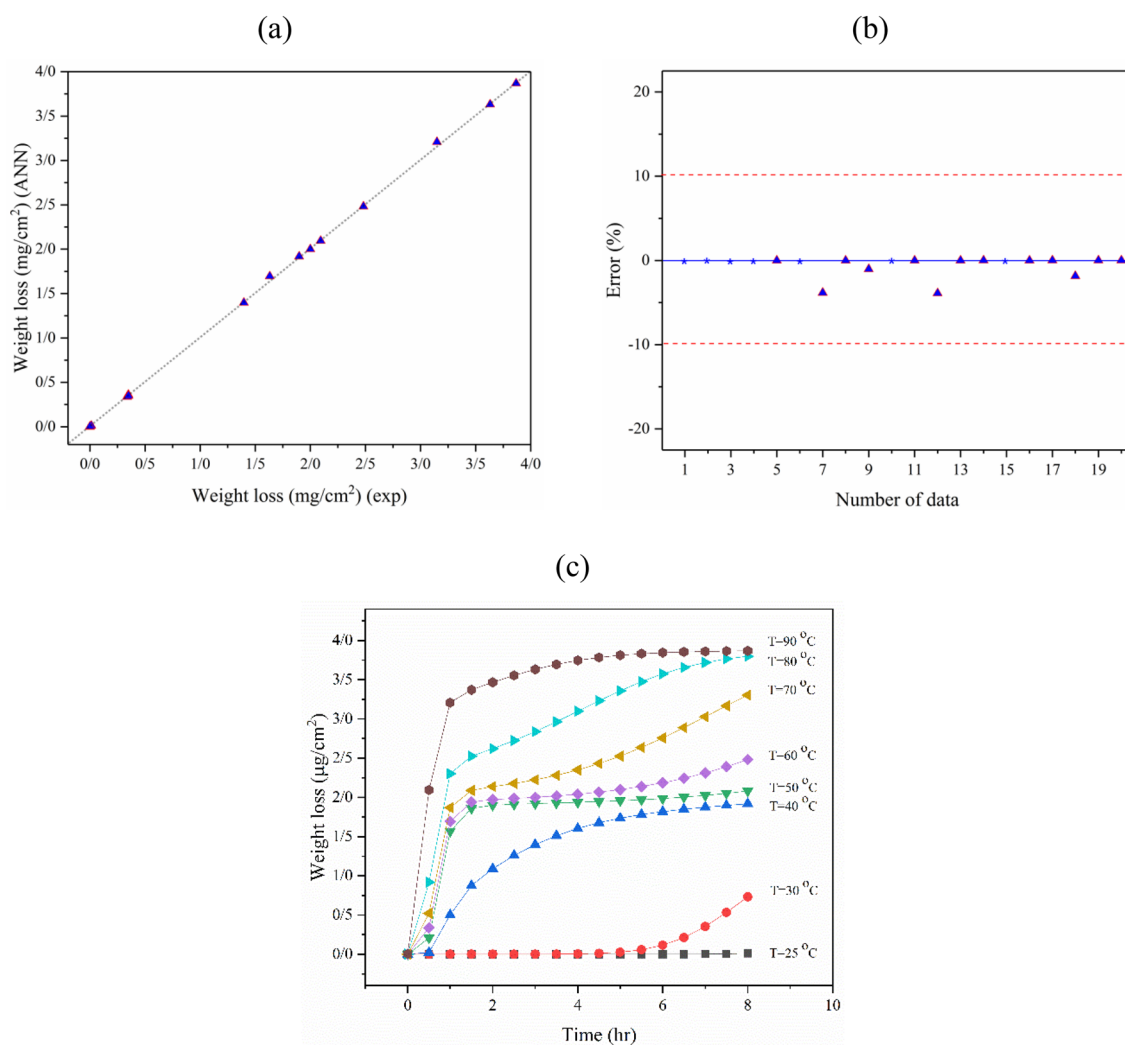
Figure 10. (**a**) Quality line, (**b**) the error values for experimental data and ANN model (R = 0.9991) outputs of WL (error for some points was unaccountable because of zero experimental values), and (**c**) the effect of time and temperature on the WL of the titanium surface after etching with an H_2SO_4 etchant solution.

tion of transfer functions for the first and second hidden layers. A schematic of the optimized ANN topology is illustrated in Fig. 9. Comparison of experimental data with ANN-based WL predictions showed good accuracy with a correlation coefficient of 0.9991. The quality line and prediction error are presented in Fig. 10a,b. Finally, the variation of titanium WL in the H_2SO_4-based etching process under different etching times and solution temperatures is shown in Fig. 10c.

NSGA-II based optimization. *Optimization of R_a and WL.* As noted previously, WL and R_a are the two main responses to the etching process. WL should be minimized because of geometric limitations. On the other

hand, studies showed that a higher R_a can improve an implant's survival rate. Higher removal torque[52] is accessible through higher R_a, while higher surface roughness is the main factor responsible for enhancing surface area. Higher surface areas can improve the chances of bone cell growth on the titanium implant surfaces[27,53]. Therefore, the main goal of the etching process is to increase the surface roughness and decrease WL simultaneously. Unfortunately, there is a tradeoff between WL and surface roughness. Higher surface roughness is achieved at longer etching times and higher etchant temperatures, but these same conditions can increase WL. High temperatures and extended etching times can damage the substrate and change its geometric parameters.

The surfaces of commercial dental implants have different surface roughnesses in the range of 0.5 to less than 4 µm[21,54,55]. Surfaces with a roughness level higher than 2 µm are very limited and commonly produced by special processes, such as laser-based surface treatment methods[55,56]. On the other hand, machined surfaces of titanium-based implants are not perfectly smooth. Machined surfaces have a roughness of about 0.5 µm. On the commercial scale, surface roughnesses in the range of 0.5–2 µm are common. Therefore, multi-objective optimization was performed to minimize WL and maximize R_a (Fig. 11a), $R_a = 0.5$ (Fig. 11b), $R_a = 1$ (Fig. 11c), $R_a = 1.5$ (Fig. 11d), and $R_a = 2$ µm (Fig. 11e). In all cases, the tradeoff between R_a and WL is evident: higher R_a values lead to higher WL, and lower WL is achieved at lower R_a.

Acid etching is a common base method for subsequent surface treatment processes, such as anodizing. Previous studies have shown that the roughness of etched surfaces is effective on the final treated surface of titanium[53,57]. Therefore, the best condition for the etching process is dependent on the treatment processes that follow it. However, some points with infinite C.D. are presented in Table 2.

As noted in Table 2, higher temperatures and longer etching times are required to achieve higher R_a values. On the other hand, the lowest WL is achieved at the lowest process temperatures and shortest etching times. Therefore, objects with infinite C.D. can lead to a point with high R_a and high WL and another point with minimized WL and very low roughness (see Table 2). As noted in the previous sections, machined titanium substrates have an R_a of about 0.5 µm. Optimizing the ANN model at $R_a = 0.5$ µm for the lowest WL value leads to operating conditions with the lowest temperature and a process time close to 0 h. Moreover, the best route to achieving a R_a value of 2 µm was an operating temperature of 54.12 °C and an etching time of 3.62 h. Under these conditions, the lowest WL achieved is about 1.96 µg/cm^2.

Optimization of R_a and R_z. Homogeneity is a target parameter for surfaces in dental implant production. Homogeneity has several effects on the characterizations of dental implant surfaces and the production process[58,59]. Achieving a perfectly reproducible product is dependent on the production of homogeneous surfaces. Variation of characteristics from point to point or product to product is very high in heterogeneous surfaces. One element of surface homogeneity is approaching the R_z to R_a. It is clear that R_z is usually much more than R_a. On the other hand, the difference between R_a and R_z is not a surface recognition factor as being heterogeneous. However, a surface with R_z close to the R_a value is considered more homogeneous than a surface with R_z far removed from the R_a value. All surfaces in this study have an R_z higher than 3 µm, which is higher than the R_a values. Figure 12a shows that the R_z of the H_2SO_4-etched titanium surface was altered from lower than 4 to about 18. The first objective was to minimize the R_z and maximize the R_a (Fig. 12a). The optimization to minimize R_z at $R_a = 0.5$, $R_a = 1$, $R_a = 1.5$, and $R_a = 2$ are presented in Fig. 12b–e. Some points with infinite C.D. and their operating conditions are noted in Table 3. From Table 3, we can see that the lowest achievable R_z is a little lower than 4 µm. At this point, a minimized R_a will be obtained. On the other hand, a maximized R_z is obtained (higher than 18 µm) under harsh process conditions that lead to the highest R_a (about 3.5 µm).

Discussion

The surface characteristics of dental implants affect the osseointegration process and implant survival rate. In this context, a surface treatment process that affects implant surface composition, surface roughness, and surface homogeneity is vital to developing new surfaces that facilitate osseointegration. This study provides a novel approach to using the ANN and NSGA-II to model and optimize the dental implant etching process. ANN optimizations, such as the one used in this study, have previously been used in other fields, such as surface roughness optimization of magnesium alloy machining[60] and finish turning of AISI 4140 hardened steel[61].

Three ANN models were developed to predict R_a, R_z, and WL based on H_2SO_4 temperature and etching duration. In agreement with previous studies, all the correlation coefficients were above 0.98. Therefore, the ANN models predicted the experimental data with a high degree of accuracy. Abbas et al.[60] showed that when the correlation coefficient of ANN model was 0.986, high accuracy of their model in predicting surface roughness was achieved. In other study, Meddour et al.[61] used an ANN model with correlation coefficient of 0.99 for R_a predicting. Therefore, the configured ANN models for R_a (R = 0.9892), R_z (R = 0.9970) and WL (R = 0.9991), are reliable. Results of this study showed that the etching process can increase the surface roughness. Lazzara et al.[62] compared the bone response of a dual-etched surface to machined implants in the human posterior maxilla. After a healing time of six months, bone contact at the etched surface and the machined surface were 72.96% and 33.98% respectively. Additionally, a unique feature was detected at the etched surface that is bone creeping along the surface. The osteoconductive effect of the etch-textured surface over the machined surface, was particularly pronounced in the softer trabecular bone. In this type of bone, the amount of bone apposition was enhanced from 6.5 ± 10.8% for the machined surface to 59.1 ± 25.3% for the etched surface.

Low removal torque is a fundamental problem in some dental implant with relatively smooth surfaces. Low removal torque can lead to in place rotation of dental implant in prosthetic loading. Higher roughness can increase needed removal torque that can be achieved by etching process in the conditions resulted in this study. Klokkevold et al.[52] investigated the anchoring of the etched and machined surfaces on rabbit tibia after one, two and three months. After one month, the mean removal torque of the machined surface was 6.00 ± 0.64 N cm,

(a)

(b)

(c)

(d)

(e)
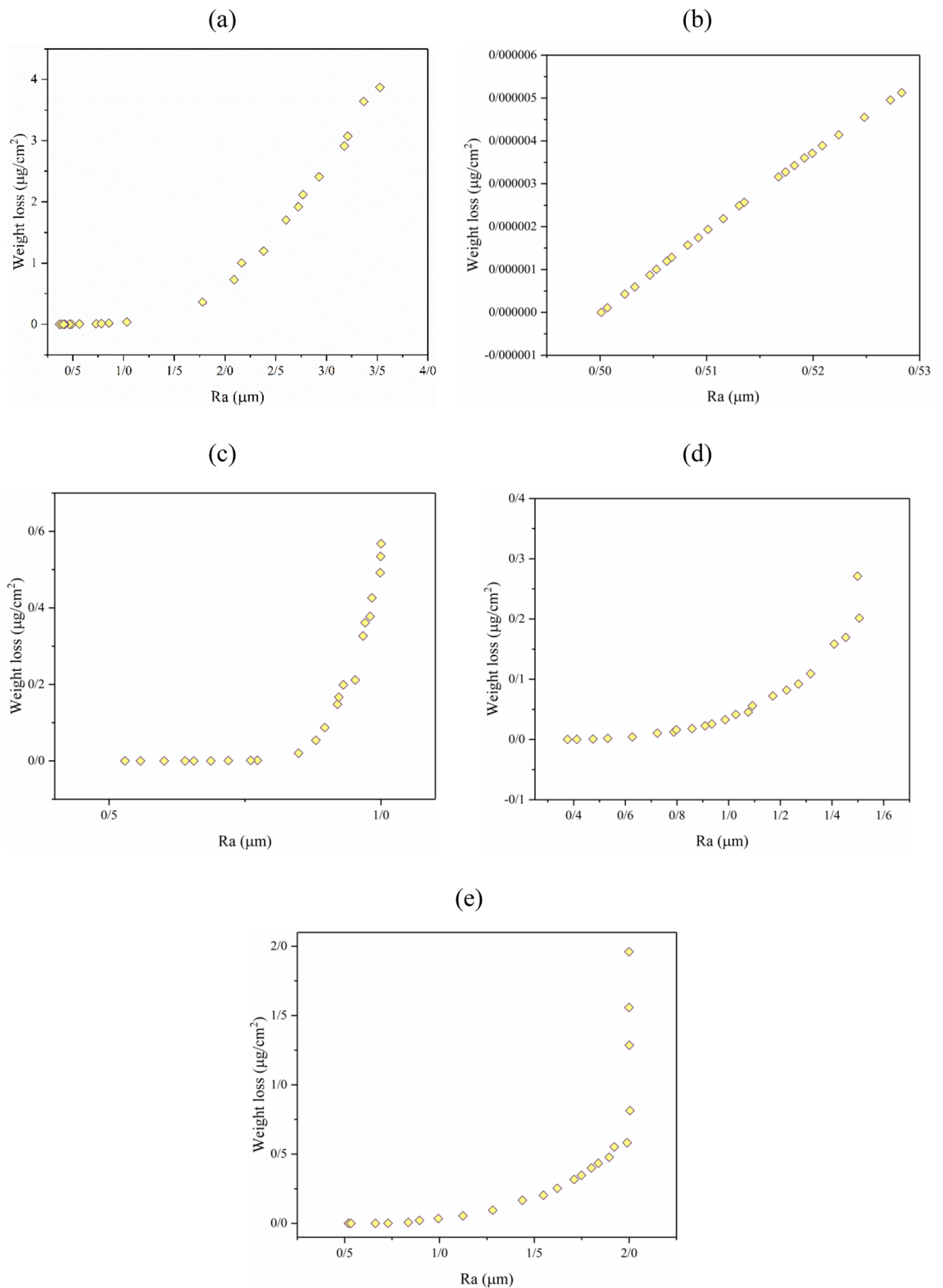
Figure 11. Multi-objective optimization of R_a and WL in the etching of titanium to (**a**) maximized R_a and minimized WL, (**b**) fixed $R_a = 0.5$ and WL minimized, (**c**) fixed $R_a = 1$ and WL minimized, (**d**) fixed $R_a = 1.5$ and WL minimized, and (**e**) fixed $R_a = 2$ μm and WL minimized.

Goal	Temperature (°C)	Time (h)	R_a (μm)	WL (μg/cm²)
R_a maximize	90.00	8.00	3.53	3.87
WL minimize	50.86	0.00	0.37	0.00
R_a = 0.5 μm	25.08	1.54	0.53	0.00
WL minimize	25.00	1.09	0.50	0.00
R_a = 1 μm	25.14	1.53	0.53	0.00
WL minimize	32.87	5.60	1.00	0.57
R_a = 1.5 μm	48.29	2.36	1.50	1.89
WL minimize	58.05	0.00	0.38	0.00
R_a = 2 μm	54.12	3.62	2.00	1.96
WL minimize	29.87	0.77	0.52	0.00

Table 2. Some optimized points with infinite C.D. for R_a–WL optimization.

whereas it was 3.6 times higher for the etched surface at 21.86 ± 1.37 N cm. After two months, the difference was 3.0 times, and after three months, the etched surface required a removal torque of 27.40 ± 3.89 N cm versus 6.73 ± 0.95 N cm for the machined surface.

To achieve a homogenous surface, the optimization conditions were needed to minimize R_z and maximize R_a. The conditions to achieve a minimum R_z at R_a = 2 μm, were considered. The most homogenous surface (a R_a to R_z ratio of about 0.2) was achieved at 90 °C after 6.26 h of etching. Etching at about 48 °C for 6.75 h, could also result in a homogenous surface with a 0.17 R_a to R_z ratio. Carvalho et al. showed that etching cpTi in 60% H_2SO_4 at 60 °C for 1 h, increased the surface isotropy of the machined surfaces from 17.4 to 91.5%[63].

Surface roughness as one of the most important parameters that is effective in dental implant performance, have been studied in this research. Reports suggest that surface roughness is not the only effective surface parameter that determines the implant's survival rate and osseous contact. Based on the clinical experiments, acid-etched titanium (SLA) promotes a greater and more rapid osseous contact when titanium-plasma-sprayed implants are used[33,64]. Surface hydrogen concentration and the formation of titanium hydride[65], surface topology[44,66] and surface wettability[67] are some other parameters that are improved through the acid etching process.

In advanced dental implant surface treatment methods like SLA, a combination of air-abrasion parameters and acid etching variables can specify the final properties of the surface. After optimizing surface roughness by varying the acid etching parameters, we will study the sandblasting process. In future studies, we are interested in exploring the effect of different sand particle shapes on the surface configurations of dental implants. In addition, gas flow velocity, pressure, temperature, particle size, size distribution, and particle nature may also influence the final surface characteristics. However, since surface properties can be altered in the etching step, the outcomes of both treatments need to be considered to achieve the most favorable results.

Conclusions

We evaluated the impact of etching solution temperature and etching process time on the surface characteristics (R_a, R_z, and WL) of dental implants in an acidic solution containing 48% H_2SO_4. The results showed that increasing both temperature and process time can enhance R_a, R_z, and WL. In addition, results confirmed the ability of an MLP-ANN model to predict the surface characteristics as a function of the etching parameters. Increasing the etching process time leads to higher R_a, R_z and WL values. Based on the MLP-ANN predictions, increasing etching time at higher etching solution temperatures is more effective for improving the surface characteristics. In the following, NSGA-II based multi-objective optimization was used for obtaining the optimum time of etching and temperature of etching solution with the aim of minimizing the W_L and R_z and maximizing the R_a. Finally, the results showed that the NSGA-II based optimization could be successfully applied for MLP-ANN based modeled etching process that could be used in dental implant surface treatment. Regarding the obtained results, ANN based models can be used for next studies of surface characteristics modelling. In addition, NSGA-II based multi-objective optimization can be successfully applied for prediction of the ideal operation condition, having the best surface.
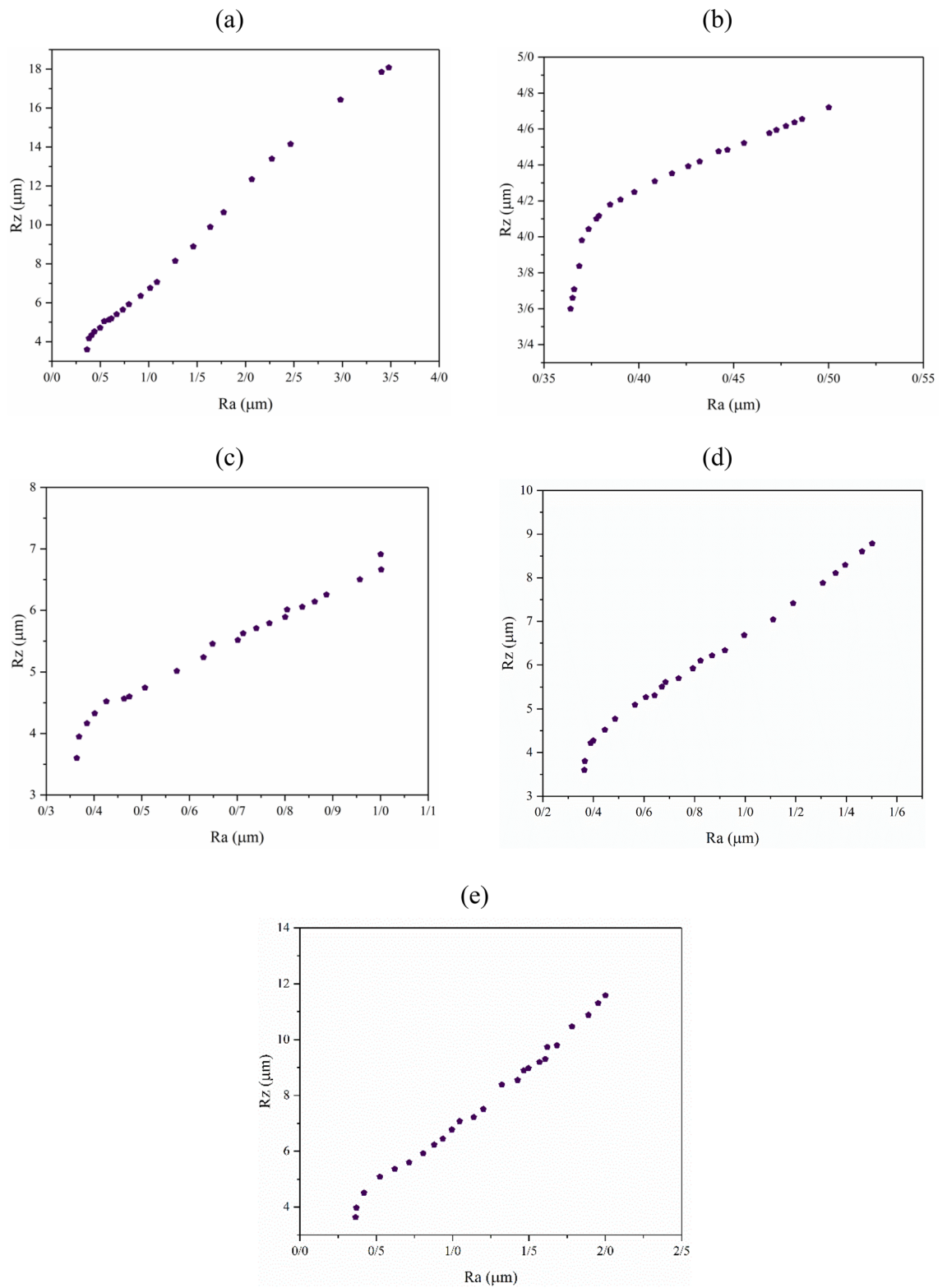
Figure 12. Multi-objective optimization of R_a and R_z in the etching of titanium to achieve (**a**) maximized R_a and minimized R_z, (**b**) fixed $R_a = 0.5$ and minimized R_z, (**c**) fixed $R_a = 1$ and minimized R_z, (**d**) fixed $R_a = 1.5$ and minimized R_z, and (**e**) fixed $R_a = 2$ μm and minimized R_z.

Goal	Temperature (°C)	Time (h)	Ra (µm)	WL (µg/cm²)
R_a maximize	25.00	0.00	0.36	3.60
R_z minimize	90.00	6.26	3.48	18.08
$R_a = 0.5$ µm	25.00	0.00	0.36	3.60
R_z minimize	25.79	0.99	0.50	4.72
$R_a = 1$ µm	36.57	3.63	1.00	6.91
R_z minimize	25.00	0.00	0.36	3.60
$R_a = 1.5$ µm	25.00	0.00	0.36	3.60
R_z minimize	37.72	8.00	1.50	8.78
$R_a = 2$ µm	48.29	6.75	2.00	11.59
R_z minimize	34.60	0.00	0.36	3.64

Table 3. Some optimized points with infinite C.D. for Ra–WL optimization.

References

1. Murr, L. E. Metallurgy principles applied to powder bed fusion 3D printing/additive manufacturing of personalized and optimized metal and alloy biomedical implants: An overview. *J. Mater. Res. Technol.* **9**, 1087–1103 (2020).
2. Priyadarshini, B. *et al.* Structural, morphological and biological evaluations of cerium incorporated hydroxyapatite sol–gel coatings on Ti–6Al–4V for orthopaedic applications. *J. Mater. Res. Technol.* **12**, 1319–1338 (2021).
3. Nazir, F., Iqbal, M., Khan, A. N., Mazhar, M. & Hussain, Z. Fabrication of robust poly L-lactic acid/cyclic olefinic copolymer (PLLA/COC) blends: Study of physical properties, structure, and cytocompatibility for bone tissue engineering. *J. Mater. Res. Technol.* **13**, 1732–1751 (2021).
4. Ansari, M., Naghib, S., Moztarzadeh, F. & Salati, A. Synthesis and characterization of hydroxyapatitecalcium hydroxide for dental composites. *Ceram. Silikaty* **55**, 123–126 (2011).
5. Duyck, J., Slaets, E., Sasaguri, K., Vandamme, K. & Naert, I. Effect of intermittent loading and surface roughness on peri-implant bone formation in a bone chamber model. *J. Clin. Periodontol.* **34**, 998–1006 (2007).
6. Samavedi, S., Whittington, A. R. & Goldstein, A. S. Calcium phosphate ceramics in bone tissue engineering: A review of properties and their influence on cell behavior. *Acta Biomater.* **9**, 8037–8045 (2013).
7. Balshe, A. A., Eckert, S. E., Koka, S., Assad, D. A. & Weaver, A. L. The effects of smoking on the survival of smooth-and rough-surface dental implants. *Int. J. Oral Maxillofac. Implants* **23**, 1117–1122 (2008).
8. Balshe, A. A., Assad, D. A., Eckert, S. E., Koka, S. & Weaver, A. L. A retrospective study of the survival of smoothand rough-surface dental implants. *Int. J. Oral Maxillofac. Implants* **24**, 1113–1118 (2009).
9. Boyle, W. J., Simonet, W. S. & Lacey, D. L. Osteoclast differentiation and activation. *Nature* **423**, 337–342 (2003).
10. Gittens, R. A. *et al.* The effects of combined micron-/submicron-scale surface roughness and nanoscale features on cell proliferation and differentiation. *Biomaterials* **32**, 3395–3403 (2011).
11. Azzola, F. *et al.* Biofilm formation on dental implant surface treated by implantoplasty: An in situ study. *Dent. J.* **8**, 40 (2020).
12. Buser, D. *et al.* Influence of surface characteristics on bone integration of titanium implants. A histomorphometric study in miniature pigs. *J. Biomed. Mater. Res.* **25**, 889–902 (1991).
13. Szmukler-Moncler, S., Reingewirtz, Y. & Weber, H. P. Bone response to early loading: The effect of surface state. *Biol. Mech. Tooth Mov. Craniofacial Adapt. Bost. Harvard Soc. Adv. Orthod.* **611**, 616 (1996).
14. Szmukler-Moncler, S., Perrin, D., Ahossi, V. & Pointaire, P. Evaluation of BONIT*, a fully resorbable CaP coating obtained by electrochemical deposition, after 6 weeks of healing: a pilot study in the pig maxilla. *Key Eng. Mater.* **192**, 395–398 (2001).
15. Zabala, A. *et al.* Quantification of dental implant surface wear and topographical modification generated during insertion. *Surf. Topogr. Metrol. Prop.* **8**, 15002 (2020).
16. da Silva Brum, I. *et al.* Ultrastructural characterization of the titanium surface degree IV in dental implant aluminum free (acid attack). *J. Biomater. Nanobiotechnol.* **11**, 151 (2020).
17. Isler, S. C. *et al.* The effects of decontamination methods of dental implant surface on cytokine expression analysis in the reconstructive surgical treatment of peri-implantitis. *Odontology* **109**, 1–11 (2020).
18. Nicolas-Silvente, A. I. *et al.* Influence of the titanium implant surface treatment on the surface roughness and chemical composition. *Materials (Basel).* **13**, 314 (2020).
19. Pintão, C. A. F., Correa, D. R. N. & Grandini, C. R. Torsion modulus as a tool to evaluate the role of thermo-mechanical treatment and composition of dental Ti–Zr alloys. *J. Mater. Res. Technol.* **8**, 4631–4641 (2019).
20. Elias, C. N., Fernandes, D. J., de Souza, F. M., dos Monteiro, E. S. & de Biasi, R. S. Mechanical and clinical properties of titanium and titanium-based alloys (Ti G2, Ti G4 cold worked nanostructured and Ti G5) for biomedical applications. *J. Mater. Res. Technol.* **8**, 1060–1069 (2019).
21. Ehrenfest, D. M. D. *et al.* Identification card and codification of the chemical and morphological characteristics of 62 dental implant surfaces. Part 1: Description of the Implant Surface Identification Standard (ISIS) codification system. *POSEIDO* **2**, 7–22 (2014).
22. Chrcanovic, B. R., Albrektsson, T. & Wennerberg, A. Bone quality and quantity and dental implant failure: A systematic review and meta-analysis. *Int. J. Prosthodont.* **30**, 219–237 (2017).
23. Chrcanovic, B. R., Kisch, J., Albrektsson, T. & Wennerberg, A. Factors influencing early dental implant failures. *J. Dent. Res.* **95**, 995–1002 (2016).
24. Elias, C. N. Titanium dental implant surfaces. *Matéria (Rio Janeiro)* **15**, 138–142 (2010).
25. Grizon, F., Aguado, E., Huré, G., Baslé, M. F. & Chappard, D. Enhanced bone integration of implants with increased surface roughness: A long term study in the sheep. *J. Dent.* **30**, 195–203 (2002).
26. Fouziya, B. *et al.* Surface modifications of titanium implants—The new, the old, and the never heard of options. *J. Adv. Clin. Res. Insights* **3**, 215–219 (2016).
27. Jemat, A., Ghazali, M. J., Razali, M. & Otsuka, Y. Surface modifications and their effects on titanium dental implants. *Biomed. Res. Int.* **2015**, 1–11 (2015).

28. Braceras, I., De Maeztu, M. A., Alava, J. I. & Gay-Escoda, C. In vivo low-density bone apposition on different implant surface materials. *Int. J. Oral Maxillofac. Surg.* **38**, 274–278 (2009).
29. Patil, P. S. & Bhongade, M. L. Dental implant surface modifications: A review. *IOSR-JDMS* **15**, 132–141 (2016).
30. Wennerberg, A. & Albrektsson, T. On implant surfaces: A review of current knowledge and opinions. *Int. J. Oral Maxillofac. Implants* **25**, 63–74 (2010).
31. Marin, C. *et al.* Removal torque and histomorphometric evaluation of bioceramic grit-blasted/acid-etched and dual acid-etched implant surfaces: An experimental study in dogs. *J. Periodontol.* **79**, 1942–1949 (2008).
32. Klokkevold, P. R., Nishimura, R. D., Adachi, M. & Caputo, A. Osseointegration enhanced by chemical etching of the titanium surface. A torque removal study in the rabbit. *Clin. Oral Implants Res.* **8**, 442–447 (1997).
33. Cho, S.-A. & Park, K.-T. The removal torque of titanium screw inserted in rabbit tibia treated by dual acid etching. *Biomaterials* **24**, 3611–3617 (2003).
34. Baker, D., London, R. M. & O'Neal, R. Rate of pull-out strength gain of dual-etched titanium implants: A comparative study in rabbits. *Int. J. Oral Maxillofac. Implants* **14**, 722–728 (1999).
35. Cochran, D. L. *et al.* The use of reduced healing times on ITI° implants with a sandblasted and acid-etched (SLA) surface: Early results from clinical trials on ITI° SLA implants. *Clin. Oral Implants Res.* **13**, 144–153 (2002).
36. Roccuzzo, M., Bunino, M., Prioglio, F. & Bianchi, S. D. Early loading of sandblasted and acid-etched (SLA) implants: A prospective split-mouth comparative study: 1-year results. *Clin. Oral Implants Res.* **12**, 572–578 (2001).
37. Testori, T. *et al.* A multicenter prospective evaluation of 2-months loaded Osseotite° implants placed in the posterior jaws: 3-year follow-up results. *Clin. Oral Implants Res.* **13**, 154–161 (2002).
38. Lazzara, R. J., Porter, S. S., Testori, T., Galante, J. & Zetterqvist, L. A prospective multicenter study evaluating loading of osseotite implants two months after placement: 1-year results. *J. Esthet. Restor. Dent.* **10**, 280–289 (1998).
39. Esfe, M. H. & Tilebon, S. M. S. Statistical and artificial based optimization on thermo-physical properties of an oil based hybrid nanofluid using NSGA-II and RSM. *Phys. A Stat. Mech. Appl.* **537**, 122126 (2020).
40. Salehi, M. M., Hakkak, F., Tilebon, S. M., Ataeefard, M. & Rafizadeh, M. Intelligently optimized electrospun polyacrylonitrile/poly (vinylidene fluoride) nanofiber: Using artificial neural networks. *Express Polym. Lett.* **14**, 1003–1017 (2020).
41. Ataeefard, M., Tilebon, S. M. S., Etezad, S. M. & Mahdavi, S. Intelligent modeling and optimization of environmentally friendly green enzymatic deinking of printed paper. *Environ. Sci. Pollut. Res.* **29**, 1–14 (2022).
42. Ataeefard, M. & Tilebon, S. M. S. Seeking a paper for digital printing with maximum gamut volume: A lesson from artificial intelligence. *J. Coat. Technol. Res.* **19**, 285–293 (2022).
43. Kohler, R., Sowards, K. & Medina, H. Numerical model for acid-etching of titanium: Engineering surface roughness for dental implants. *J. Manuf. Process.* **59**, 113–121 (2020).
44. Ban, S., Iwaya, Y., Kono, H. & Sato, H. Surface modification of titanium by etching in concentrated sulfuric acid. *Dent. Mater.* **22**, 1115–1120 (2006).
45. Ataeefard, M., Sadati Tilebon, S. M. & Saeb, M. R. Intelligent modeling and optimization of emulsion aggregation method for producing green printing ink. *Green Process. Synth.* **8**, 703–718 (2019).
46. Hekmatjoo, N. *et al.* Modeling of glycolysis of flexible polyurethane foam wastes by artificial neural network methodology. *Polym. Int.* **64**, 1111–1120 (2015).
47. Xu, Y., Zhu, Y., Xiao, G. & Ma, C. Application of artificial neural networks to predict corrosion behavior of Ni–SiC composite coatings deposited by ultrasonic electrodeposition. *Ceram. Int.* **40**, 5425–5430 (2014).
48. Tilebon, S. M. S. & Norouzbeigi, R. Anti-icing nano SnO$_2$ coated metallic surface wettability: Optimization via statistical design. *Surf. Interfaces* **21**, 100720 (2020).
49. Yousefi, H. & Fallahnezhad, M. Multi-objective higher order polynomial networks to model insertion force of bevel-tip needles. *Int. J. Nat. Comput. Res.* **5**, 54–70 (2015).
50. Fallahnezhad, M. & Yousefi, H. Needle insertion force modeling using genetic programming polynomial higher order neural network. In *Artificial Higher Order Neural Networks for Modeling and Simulation* (ed. Zhang, M.) 58–76 (IGI Global, 2013).
51. Ataeefard, M., Tilebon, S. M. S. & Saeb, M. R. Intelligent modeling and optimization of emulsion aggregation method for producing green printing ink. *Green Process. Synth.* **8**, 703–718 (2019).
52. Klokkevold, P. R. *et al.* Early endosseous integration enhanced by dual acid etching of titanium: A torque removal study in the rabbit. *Clin. Oral Implants Res.* **12**, 350–357 (2001).
53. Matos, G. R. M. Surface roughness of dental implant and osseointegration. *J. Maxillofac. Oral Surg.* **20**, 1–4 (2021).
54. Ehrenfest, D. M. D. *et al.* Identification card and codification of the chemical and morphological characteristics of 62 dental implant surfaces. Part 3: Sand-blasted/acid-etched (SLA type) and related surfaces (group 2A, main subtractive process). *POSEIDO* **2**, 37–55 (2014).
55. Dohan Ehrenfest, D. M., Vazquez, L., Park, Y.-J., Sammartino, G. & Bernard, J.-P. Identification card and codification of the chemical and morphological characteristics of 14 dental implant surfaces. *J. Oral Implantol.* **37**, 525–542 (2011).
56. Kalemaj, Z., Scarano, A., Valbonetti, L., Rapone, B. & Grassi, F. R. Bone response to four dental implants with different surface topographies: A histologic and histometric study in Minipigs. *Int. J. Periodont. Restor. Dent.* **36**, 745–754 (2016).
57. Alla, R. K. *et al.* Surface roughness of implants: A review. *Trends Biomater. Artif. Organs* **25**, 112–118 (2011).
58. Mendonça, G., Mendonça, D. B. S., Aragao, F. J. L. & Cooper, L. F. Advancing dental implant surface technology—From micron-to nanotopography. *Biomaterials* **29**, 3822–3835 (2008).
59. Pelaez-Vargas, A. *et al.* Isotropic micropatterned silica coatings on zirconia induce guided cell growth for dental implants. *Dent. Mater.* **27**, 581–589 (2011).
60. Abbas, A. T. *et al.* ANN surface roughness optimization of AZ61 magnesium alloy finish turning: Minimum machining times at prime machining costs. *Materials (Basel).* **11**, 808 (2018).
61. Meddour, I., Yallese, M. A., Bensouilah, H., Khellaf, A. & Elbah, M. Prediction of surface roughness and cutting forces using RSM, ANN, and NSGA-II in finish turning of AISI 4140 hardened steel with mixed ceramic tool. *Int. J. Adv. Manuf. Technol.* **97**, 1931–1949 (2018).
62. Lazzara, R. J., Testori, T., Trisi, P., Porter, S. S. & Weinstein, R. L. A human histologic analysis of osseotite and machined surfaces using implants with 2 opposing surfaces. *Int. J. Periodont. Restor. Dent.* **19**, 117–129 (1999).
63. de Carvalho, D. R. *et al.* Characterization and in vitro cytocompatibility of an acid-etched titanium surface. *Braz. Dent. J.* **21**, 3–11 (2010).
64. Ogawa, T. *et al.* Biomechanical evaluation of osseous implants having different surface topographies in rats. *J. Dent. Res.* **79**, 1857–1863 (2000).
65. Conforto, E., Caillard, D., Aronsson, B. O. & Descouts, P. Electron microscopy on titanium implants for bone replacement after "SLA" surface treatment. *Eur. Cells Mater.* **3**, 9–10 (2002).
66. Perrin, D., Szmukler-Moncler, S., Echikou, C., Pointaire, P. & Bernard, J.-P. Bone response to alteration of surface topography and surface composition of sandblasted and acid etched (SLA) implants. *Clin. Oral Implants Res.* **13**, 465–469 (2002).
67. Ponsonnet, L. *et al.* Relationship between surface properties (roughness, wettability) of titanium and titanium alloys and cell behaviour. *Mater. Sci. Eng. C* **23**, 551–560 (2003).

Author contributions

S.M.S.T. performed the analyses. S.A.E.S., H.R., H.Y., M.O. and S.M.N. established the main idea as well as wrote and edited the main manuscript text. Y.Z. and K.Y.R. edited the manuscript.

Competing interests

The authors declare no competing interests.

Additional information

Correspondence and requests for materials should be addressed to S.M.N.

Reprints and permissions information is available at www.nature.com/reprints.

Publisher's note Springer Nature remains neutral with regard to jurisdictional claims in published maps and institutional affiliations.